The Active Site of *Paracoccus denitrificans* Aromatic Amino Acid Aminotransferase Has Contrary Properties: Flexibility and Rigidity[†,‡]

Akihiro Okamoto,[§] Seiji Ishii,[§] Ken Hirotsu,[||] and Hiroyuki Kagamiyama*[,§]

Department of Biochemistry, Osaka Medical College, Takatsuki, Osaka 569-8686, Japan, and Department of Chemistry, Faculty of Science, Osaka City University, Sumiyoshi-ku, Osaka 558-8585, Japan

Received August 10, 1998; Revised Manuscript Received November 9, 1998

ABSTRACT: *Paracoccus denitrificans* aromatic amino acid aminotransferase (EC 2.6.1.57; pdAroAT) binds with a series of aliphatic monocarboxylates attached to the bulky hydrophobic groups. To analyze the properties of the active site in this enzyme, we determined the tertiary structures of pdAroAT complexed with nine different inhibitors. Comparison of these active site structures showed that the active site of pdAroAT consists of two parts with contrary properties: rigidity and flexibility. The regions that interact with the carboxylates and methylene chains of the inhibitors gave essentially the same structures among these complexes, exhibiting the rigid property, which would involve fixing the substrate at the proper orientation for efficient catalysis. The region that interacts with the terminal hydrophobic groups of the inhibitors gave versatile structures according to the structures of the terminal groups, showing that this region is structurally flexible. This is mainly achieved by the conformational versatility of the side chains of Asp15, Lys16, Asn142, Arg292*, and Ser296*. These residues formed in the active site hydrogen bond networks, which were adaptable for the structures of the terminal hydrophobic groups of the inhibitors, with a small deformation or partial destruction according to the shapes and sizes of the inhibitors. These observations illustrate how the flexibility and rigidity in the active site can be used for the substrate binding and recognition.

Many enzymes alter their active sites and entire structures upon binding of the substrate to make intimate interactions between the enzyme and substrate. These structural changes were called "induced fit" by Koshland and closely correlated with the substrate specificity of the enzyme. The conformational changes and flexibility of the enzymes that alter the entire structures upon binding of the substrate were extensively reviewed and classified (*1*), but systematic studies of the conformational changes and flexibility observed for the active site structures are very limited. Morton et al. studied the role of shape complementarity in nonpolar ligand binding with a mutant T4 lysozyme containing a cavity in a protein core (*2*, *3*). They thermodynamically studied binding of the 91 different ligands to the cavity of the mutant and estimated the energetic origins of specificity of the ligand binding. In addition, they determined the tertiary structures of the enzymes complexed with nine ligands and showed that the cavity consists of two parts that respond very differently to the binding of ligands: rigid and flexible regions. They suggested that the relatively rigid region may be responsible for determining the ligand specificity, and a more flexible region may allow some versatility in the structures of the binding ligands. To extend their new observations about the artificial ligand-binding site of the mutant T4 lysozyme into the natural one of the enzyme, we studied the dynamic aspect of the active site of aromatic amino acid aminotransferase from *Paracoccus denitrificans* (EC 2.6.1.57; pdAroAT) on binding with a series of inhibitors.

pdAroAT, the pyridoxal 5′-phosphate (PLP)[1]-dependent enzyme, catalyzes the transamination reaction with both acidic and aromatic amino acid as the substrate (*4*). From the X-ray studies of the ligand−enzyme complexes, we found that this unique multiple recognition of entirely different side chains of substrates was achieved by the reconstruction of the active site, in which the side chains of Asp15, Lys16, Asn142, Arg292*, and Ser296* changed their conformations, making new hydrogen bond networks to fit the shape and property of the active site to the structures of the side chains of the binding substrates without changing the backbone movement of the active site (*5*). Thus, the flexibility of the side chains of these residues plays a major role in switching the mode of recognition for the acidic and aromatic substrates in pdAroAT. Therefore, pdAroAT is a good subject to study the role of the rigidity and flexibility of the active site in the

[†] This research was supported by a Research Grant from the Japan Society for the Promotion of Science (RFTF96L00506).

[‡] Coordinates have been deposited in the Brookhaven Protein Data Bank.

* To whom correspondence should be addressed. E-mail: med001@art.osaka-med.ac.jp. Fax: +81-726-84-6516.

[§] Osaka Medical College.

[||] Osaka City University.

[1] Abbreviations: ASA, accessible surface area; AroAT, aromatic amino acid aminotransferase; pdAroAT, AroAT from *Paracoccus denitrificans*; AspAT, aspartate aminotransferase; PP, 3-phenylpropionic acid; IP, 3-indolepropionic acid; IB, 3-indolebutyric acid; PB, 4-phenylbutyric acid; PV, 5-phenylvaleric acid; TB, 4-(2-thienyl)butyric acid; CHP, cyclohexanepropionic acid; AHC, 4-aminohydrocinnamic acid; PTP, 3-(p-tolyl)propionic acid; DMP, 3-(3,4-dimethoxyphenyl)propionic acid; PLP, pyridoxal 5′-phosphate; rms, root-mean-square; Arg292*, * indicating a residue from the neighboring subunit of the catalytic active dimer.

10.1021/bi981921d CCC: $18.00
Published on Web 01/08/1999

Table 1: Data Collection

inhibitor[a]	AHC	CHP	DMP	PTP	IP	TB	PB	IB	PV
lattice const.									
a (Å)	124.14	123.95	123.87	124.20	124.00	123.78	124.08	124.01	123.78
b (Å)	121.74	121.86	121.69	121.79	122.06	121.32	121.79	121.78	120.94
c (Å)	55.20	55.20	55.23	55.17	55.11	54.92	55.21	55.13	54.90
no. of rflns	90 361	86 693	81 817	96 560	74 845	107 781	76 988	103 406	84 921
no. of unique rflns	30 812	27 153	26 603	31 319	22 591	33 737	24 918	32 656	28 356
completeness (%)	96.0	97.7	99.1	98.1	96.9	98.3	98.0	98.5	96.5
resolution limit (Å)	2.2	2.4	2.4	2.2	2.4	2.2	2.4	2.2	2.4
R_{merge}[b] (%)	9.3	6.2	8.5	6.6	8.0	6.8	7.4	7.2	10.7

[a] See text for abbreviations of the inhibitors. [b] $R_{merge} = \Sigma_i|I_i - \langle I_i\rangle|/\Sigma_i\langle I_i\rangle$ where I_i is the intensity of an individual reflection and $\langle I_i\rangle$ is the mean intensity of that reflection.

substrate binding and specificity. We kinetically analyzed the binding of the various aliphatic monocarboxylates attached to the bulky hydrophobic groups to the active site, and crystallographically determined the tertiary structures of pdAroAT complexed with nine kinds of inhibitors: 3-indolepropionic acid (IP), 3-indolebutyric acid (IB), 4-phenylbutyric acid (PB), 5-phenylvaleric acid (PV), 4-(2-thienyl)butyric acid (TB), cyclohexanepropionic acid (CHP), 4-aminohydrocinnamic acid (AHC), 3-(p-tolyl)propionic acid (PTP), and 3-(3,4-dimethoxyphenyl)propionic acid (DMP).

MATERIALS AND METHODS

Materials. pdAroAT was prepared as described previously (*5*). CHP, cyclohexanebutyric acid, cyclopentylpropionic acid, DMP, 3-(2-hydroxyphenyl)propionic acid, 3-(2-methoxyphenyl)propionic acid, 3-(3-methoxyphenyl)propionic acid, 3-(4-methoxyphenyl)propionic acid, 4-(4-nitrophenyl)-butyric acid, 1-piperidinepropionic acid, PTP, PV, TB, and 3-(3,4,5-trimethoxyphenyl)propionic acid were purchased from Aldrich (Milwaukee, WI). AHC, IP, and 2,4,6-tricholorophenoxyacetic acid were from Tokyo Kasei (Tokyo, Japan). IB and PB were from Nacalai Tesque (Kyoto, Japan). 3-Indoleacetic acid and 4-pentenoic acid were from Wako Pure Chemicals (Osaka, Japan). All other chemicals were of the highest purity available.

Spectroscopic Measurements. The absorption spectra of the inhibitor complexes of pdAroAT were measured using a Hitachi U-3300 spectrophotometer at 25 °C. The buffer solution contained 50 mM HEPES−NaOH and 0.1 M KCl (pH 7.5). The final enzyme concentration was 10 μM.

Crystallizations. Structural formulas of nine kinds of inhibitors and 3-phenylpropionic acid (PP), which were used for the X-ray analyses of the enzyme−inhibitor complexes, are shown in Figure 1. Crystals of the enzyme−inhibitor complexes, except for the CHP complex, were essentially made by the soaking method as previously described (*5*). Initially, crystals of the maleate complex of pdAroAT were made by the micro-seeding method using a precipitating buffer (24.0% (w/v) poly(ethylene glycol) 4000 in 0.2 M sodium maleate buffer (pH 5.7) containing 5 mM $MgCl_2$). To replace the cocrystallized inhibitor, maleate, with other inhibitors, we soaked the crystals in a stabilizing solution (24.0% poly(ethylene glycol) 4000 in 0.1 M sodium citrate buffer (pH 5.7)) containing 0.1 M inhibitor for tens of hours (for PTP and PV complexes, pHs of the stabilizing solutions were 6.2 and 6.5, respectively). The CHP complex of pdAroAT was crystallized in a similar manner for the crystallization of the maleate complex using a precipitating buffer (24.0% poly(ethylene glycol) 4000 in 0.1 M sodium citrate buffer (pH 6.4)) containing 0.1 M CHP.

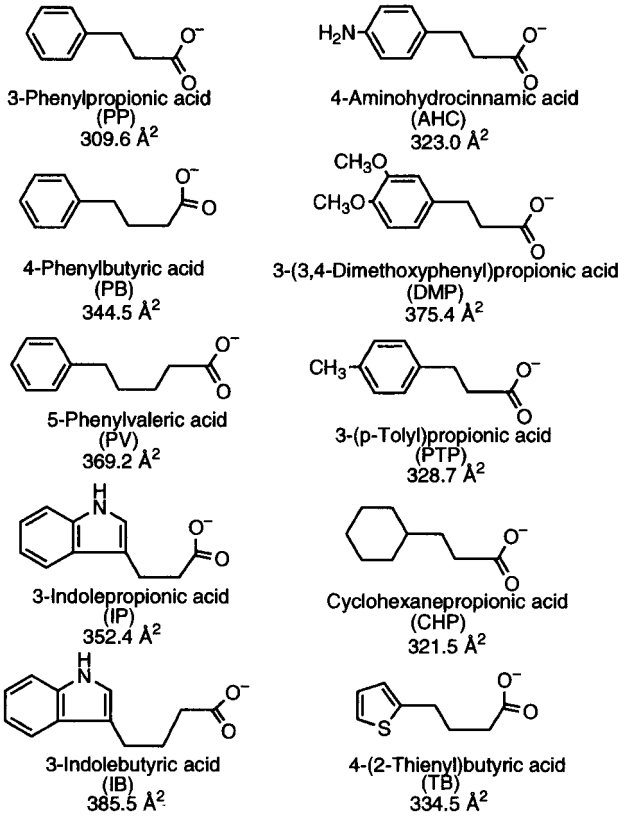

FIGURE 1: Structural formulas and accessible surface areas of inhibitors used for X-ray analyses of enzyme−inhibitor complexes.

Data Collections. All crystals belonging to the orthorhombic space group $P2_12_12_1$ showed almost identical unit cell parameters (Table 1). The X-ray diffraction data were collected with a Rigaku R-AXIS IIc image plate detector mounted on a Rigaku RU-200 rotating anode generator operated at 40 kV and 100 mA with monochromatized Cu $K\alpha$ radiation at room temperature. Each data collection was performed using one crystal. The oscillation images were processed and reduced using the data processing software Rigaku PROCESS (*6*). Statistics for the data collection are also summarized in Table 1.

Determination of the Structure. Refinements of the structures for the inhibitor complexes of pdAroAT were started with the PP complex structure of pdAroAT (*5*) as the initial model using X-PLOR (*7*) with parameters derived by Engh and Huber (*8*). After the initial conventional positional refinement, simulated annealing using the slow cool protocol

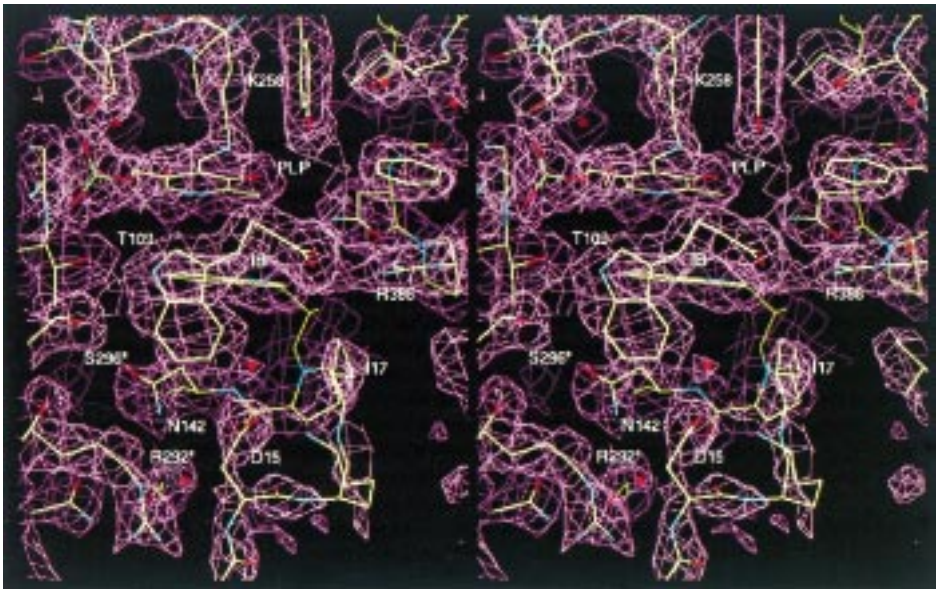

FIGURE 2: Electron density ($2F_o - F_c$ map contoured at 1σ) of the IB complex of pdAroAT, showing the active site residues, IB, and PLP. This figure was generated using the program Xfit (*9*).

Table 2: Refinement Statistics

inhibitor[a]	AHC	CHP	DMP	PTP	IP	TB	PB	IB	PV
resolution range (Å)	6.0−2.2	6.0−2.4	6.0−2.4	6.0−2.2	6.0−2.4	6.0−2.2	6.0−2.4	6.0−2.2	6.0−2.5
no. of rflns	28 583	25 002	24 376	29 073	20 535	31 474	22 760	30 410	23 545
no. of protein atoms	5983	5982	6001	5983	5985	5993	5983	5986	5997
no. of solvent atoms	290	269	325	288	272	312	250	267	189
R_{cryst}[b] (%)	18.7	17.5	16.8	18.7	16.7	19.0	17.1	20.0	18.5
R_{work} (%)	17.9	16.6	16.4	18.1	16.1	18.2	15.7	19.2	17.5
R_{free} (%)	24.0	23.4	22.1	23.0	21.8	24.5	21.9	25.8	25.3
rms dev. from ideality									
bond lengths (Å)	0.006	0.006	0.007	0.006	0.006	0.006	0.006	0.007	0.007
bond angles (deg)	1.2	1.2	1.3	1.2	1.2	1.3	1.3	1.3	1.3
improper angles (deg)	1.14	1.13	1.21	1.18	1.18	1.22	1.16	1.22	1.26
dihedrals (deg)	22.9	22.8	23.2	22.7	22.7	23.1	22.8	22.9	23.3
averaged *B* factor									
carboxylate[c] (Å^2)	21.7	43.5	20.8	20.5	25.4	26.3	26.3	19.2	28.1
probe[d] (Å^2)	22.9	44.8	20.2	20.6	24.9	27.2	19.5	20.1	33.8
active site[e] (Å^2)	24.0	26.7	22.2	25.6	22.3	25.9	23.8	23.5	25.8

[a] See text for abbreviations of the inhibitors. [b] $R_{cryst} = \Sigma|F_{obs} - F_{calc}|/\Sigma|F_{obs}|$. [c] Averaged *B* factor of the carboxylate and methylene attached to it in the inhibitor of subunit B. [d] Averaged *B* factor of the inhibitor except for the carboxylate and methylene attached to it in subunit B. [e] Averaged *B* factor of the active site residues in subunit B (atoms within a radius of 12 Å from the inhibitor).

was performed. Furthermore, the models were improved by conventional positional refinement, the isotropic *B* factor refinement, and manual rebuilding using Xfit (*9*) on the omit map calculated with the coefficients $|F_o| - |F_c|$. After the *R* factors were adequately lowered, water molecules were added to the models and the structures were further refined. Finally a complete polypeptide chain of subunits A and a polypeptide chain of subunits B without residues from 25 to 30 were modeled for all of the inhibitor complexes. The overall mean errors associated with the atomic coordinates were estimated using a Luzzati plot (*10*). The estimated positional errors were less than 0.24 Å. Two cis proline residues were observed at residues 138 and 195 of each subunit. Ramachandran plots showed that Lys16, Ala71, and Ser296 of each subunit fell outside of the energetically favorable regions, but these residues were located at or near the active site and were clearly shown in the electron density maps. Figure 2 shows the $2F_o - F_c$ electron density map contoured at 1σ for the active site of the IB complex. The detailed summaries of the refinements are given in Table 2, and the coordinates of the refined structures have been deposited with the Brookhaven Protein Data Bank (entry codes 2AY1, 2AY2, 2AY3, 2AY4, 2AY5, 2AY6, 2AY7, 2AY8, and 2AY9 for the AHC, CHP, DMP, PTP, IP, IB, PB, TB, and PV complexes, respectively).

Data Analysis. The accessible surface area (ASA) was calculated by the method of Sharke and Ruply (*11*). The secondary structures were assigned by the program DSSP (*12*). Previously determined structures of the unliganded pdAroAT and the PP complex (*5*) (PDB entry codes: 1AY4 and 1AY8, respectively) were used for discussion.

RESULTS

Dissociation Constants for the Inhibitors. The inhibitors used have the following structural features: carboxyl group at one end, versatile functional group at another end ("probing group"), and a linear aliphatic chain with 1−4 methylene groups joining them (except for ether linkage of

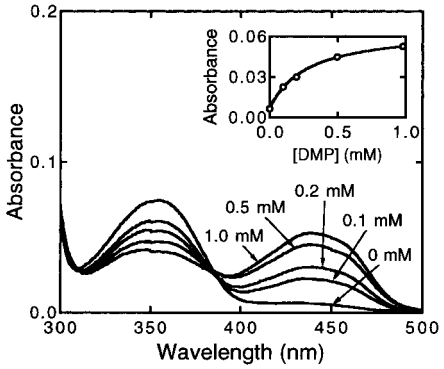

FIGURE 3: Absorption spectra of pdAroAT in the presence of DMP. Concentrations of DMP used were 0, 0.1, 0.2, 0.5, and 1.0 mM. The spectra were taken in 50 mM HEPES−NaOH buffer, pH 7.5, containing 0.1 M KCl. Inset is a titration curve of absorption at 435 nm (○). The line is the theoretical curve.

2,4,6-tricholorophenoxyacetic acid). Noncovalent binding of these inhibitors to the active site of pdAroAT shifted the pK_a of the imine of the internal aldimine bond between the pyridoxal 5′-phosphate and Lys258 to a higher value, converting the absorption band of pdAroAT from 356 nm (the unprotonated species) to 435 nm (the protonated species) (*4*). Therefore, the dissociation constants (K_d) for the inhibitors were determined by measuring the increase in the absorption at 435 nm. The bindings of the inhibitors to the enzyme showed a simple binding reaction (Figure 3). Table 3 summarizes the dissociation constants for the inhibitors, showing that pdAroAT is able to accommodate the different shape and size of the terminal "probing group". 1-Piperidinepropionic acid ($(C_5H_{10}N)(CH_2)_2COOH$), phenoxyacetic acid ($(C_6H_5)OCH_2COOH$), and 4-pentenoic acid ($CH_2{=}CH(CH_2)_2COOH$) did not show any spectral changes up to 10 mM inhibitor concentrations.

Overall Structures of the Inhibitor Complexes of pdAroAT. The pdAroAT molecule has an α_2 dimeric structure of the subunit consisting of 394 amino acid residues and one PLP as its coenzyme (*4*). One enzyme molecule resided in the crystallographic asymmetric unit, and the two subunits (subunits A and B) were related by a noncrystallographical 2-fold axis. The subunit is divided into two domain structures, a small (residues 5−48 and 326−409) and a large (residues 49−325) domain. Upon binding of the inhibitor, the small domain moved to close the active site (open−closed conformational change) (*5*). Although there are two active sites in one pdAroAT molecule, the inhibitor was found only in the active site of subunit B except for the DMP, TB, and PV complexes, in which inhibitors were bound to the active sites of both subunits. Subunits A of all of the inhibitor complexes had the open forms, in which the active sites were exposed to the solvent environment, while all subunits B had the closed forms. In subunit A, the regions which interact with the neighboring molecules by the crystal packing were two times larger than that observed in subunit B, and it would prevent subunit A from changing to the closed conformation (*5*). We then used only subunits B for the following analyses.

The superimpositions of subunits B of 10 inhibitor complexes by fitting the 266 C_α atoms of the large domains showed that all of these large domains had an identical structure with root-mean-square (rms) deviations of 0.117−0.194 Å (Figure 4). However, the small domain showed some structural differences in these complexes. These differences were similar to, but smaller than, that observed in the open-closed conformational change upon binding of the inhibitor (rms deviations of C_α atoms of the subunits are 0.167−0.571 Å between the complexes, and 1.23 Å between the open and the closed forms) (*5*). The PP, DMP, and IB complexes were in the most, and the CHP and TB complexes were in the least closed forms. The extent of the structural changes in the small domains showed no correlation with the accessible surface area of the inhibitors, the crystallization conditions, and the lattice constants. In the crystal lattices, the large domains of subunits B of all of the enzyme−inhibitor complexes were located at the same position with the same orientation, while the small domains of subunits B deviated slightly from each other, revealing that these structural changes would be caused not by the crystal packing, but by

Table 3: Dissociation Constants for the Inhibitors

inhibitor	formula	K_d (mM)[a]
3-indoleacetic acid	$(C_8H_7N)CH_2COOH$	14 (1)
3-indolepropionic acid	$(C_8H_7N)(CH_2)_2COOH$	2.6 (0.3)
3-indolebutyric acid	$(C_8H_7N)(CH_2)_3COOH$	0.78 (0.06)
3-phenylpropionic acid	$(C_6H_5)(CH_2)_2COOH$	3.9 (0.3)[b]
4-phenylbutyric acid	$(C_6H_5)(CH_2)_3COOH$	5.0 (0.3)
5-phenylvaleric acid	$(C_6H_5)(CH_2)_4COOH$	6.9 (0.5)
4-(2-thienyl)butyric acid	$(C_4H_4S)(CH_2)_3COOH$	5.8 (0.6)
4-(4-nitrophenyl)butyric acid	$NO_2(C_6H_4)(CH_2)_3COOH$	4.1 (0.9)
cyclopentylpropionic acid	$(C_5H_9)(CH_2)_2COOH$	28 (1)
cyclohexanepropionic acid	$(C_6H_{11})(CH_2)_2COOH$	13.1 (0.8)
cyclohexanebutyric acid	$(C_6H_{11})(CH_2)_3COOH$	9.0 (0.5)
4-aminohydrocinnamic acid	$NH_2(C_6H_4)(CH_2)_2COOH$	5.14 (0.09)
3-(p-tolyl)propionic acid	$CH_3(C_6H_4)(CH_2)_2COOH$	1.24 (0.04)
3-(2-hydroxyphenyl)propionic acid	$HO(C_6H_4)(CH_2)_2COOH$	16.2 (0.8)
3-(4-hydroxyphenyl)propionic acid	$HO(C_6H_4)(CH_2)_2COOH$	1.1 (0.003)[b]
3-(2-methoxyphenyl)propionic acid	$CH_3O(C_6H_4)(CH_2)_2COOH$	3.3 (0.1)
3-(3-methoxyphenyl)propionic acid	$CH_3O(C_6H_4)(CH_2)_2COOH$	1.09 (0.01)
3-(4-methoxyphenyl)propionic acid	$CH_3O(C_6H_4)(CH_2)_2COOH$	4.4 (0.4)
3-(3,4-dimethoxyphenyl)propionic acid	$(CH_3O)_2(C_6H_3)(CH_2)_2COOH$	0.28 (0.03)
3-(3,4,5-trimethoxyphenyl)propionic acid	$(CH_3O)_3(C_6H_2)(CH_2)_2COOH$	1.43 (0.05)
2,4,6-tricholorophenoxyacetic acid	$Cl_3(C_6H_2)OCH_2COOH$	8.1 (0.3)

[a] Standard deviations are shown in parentheses. [b] Taken from Oue et al. (*4*).

FIGURE 4: Stereoview superimposition of the subunits B of all inhibitor complexes and unliganded form of pdAroAT. C_α atoms (266) in the large domain are superimposed. The unliganded form is represented by the broken line and PLP by the ball-and-stick model. Residues 25−30 in all complexes are missing. This figure was generated using the program MORSCRIPT (*26*).

the differences in the structures and properties of the inhibitors.

Structures of the Inhibitors in the Active Sites. The inhibitors used for the structural analyses of the enzyme−inhibitor complexes have K_d values in solution between 0.28 mM (DMP) and 13.1 mM (CHP). Crystals of these complexes, except for the CHP complex, were made by the soaking method in solutions of 100 mM inhibitor. Averaged *B* factors of the carboxyl and probing sides of the inhibitors in subunit B were similar to those of the active site residues around the inhibitor for each of the enzyme−inhibitor complexes except for the CHP complex (Table 2), showing that ligand saturation in subunit B had been achieved in every crystal except for the CHP. The averaged *B* factor of the CHP was higher than that of the active site residues around the inhibitor, showing that CHP may bind partially to the active site.

The inhibitors can be divided into three groups by the length of the methylene chains: propionic, butyric, and valeric acid derivatives.

Figure 5A shows the superimposition of the active sites of the PP, DMP, AHC, and PTP complexes. These inhibitors have the common structure of phenylpropionic acid. Although their phenyl rings are substituted differently, these inhibitors occupied the same position with the well-overlapping phenyl rings.

Figure 5B shows the superimposition of the active sites of the PP, CHP, and IP complexes. PP, CHP, and IP are the 3-phenyl, 3-cyclohexyl, and 3-indolyl derivatives of propionic acid, respectively. Despite the significant differences in the structures of their "probing groups", these inhibitors occupied a very similar position with the well-overlapping "probing groups".

Figure 5C shows the superimposition of the active sites of the TB, PB, and IB complexes. TB, PB, and IB are the 4-thienyl, 4-phenyl, and 4-indolyl derivatives of butyric acid, respectively. Despite the structural differences in the "probing groups", these inhibitors were also located at a very similar position with the well-overlapping "probing groups".

Each superimposition showed that the inhibitors with the same methylene chain length well overlapped the carboxylate and methylene moieties. As a consequence, the positional freedom of the "probing groups" of these inhibitors would be restricted in the active site.

Figure 5D shows the superimposition of the active sites of the PP, PB, and PV complexes. These inhibitors have methylene chains with different lengths (2, 3, and 4 methylene groups in PP, PB, and PV, respectively), with a common "probing group" phenyl ring. The carboxyl groups of these inhibitors overlapped well with each other, but the positions of the phenyl groups deviated according to the length of the aliphatic moieties; the longer the methylene chain of the inhibitors, the further the phenyl rings were located from PLP.

Structures of the Active Sites. PLP is the reaction center of this enzyme. The crystallographically determined structures showed that the conformations and positions of PLP were essentially identical in all of the complexes. PLP was bound to N_ζ of Lys258 to form the internal aldimine bond. A number of hydrogen bonds or salt bridges between PLP and the protein bound PLP to the active site as observed previously (*5*). The conformations around the P−O4P and O4P−C5A bonds were the sterically favored staggered and trans ones, respectively. O1P−P−O4P−C5A was in a gauche conformation. The torsion angle around the C5A−C5 belonged to the nearly eclipsed conformation. Thus, O4P protruded toward the Trp140 side of the pyridine ring. The pyridine ring of PLP and the indole ring of Trp140 made good van der Waals stacking.

The spatial arrangements of the residues around the carboxylate and methylene chain of the inhibitors were quite similar in all of the complexes. The carboxyl group of each inhibitor formed a salt bridge with the guanidino group of Arg386 with "end-on" geometry (Figure 6). The inhibitor carboxylate oxygens also formed hydrogen bonds with the amide nitrogen of Asn194, the backbone amide group of Gly38, and the side chain nitrogen of Trp140. In addition, a water molecule formed hydrogen bonds to the N_ϵ of Arg386 and the backbone carbonyl oxygens of Leu35, Gly36, and Arg386 as shown in Figure 6, and these hydrogen bonds and the van der Waals contacts with the hydrophobic side chains of Ile17, Phe360, and Val382 held the salt bridge between Arg386 and the inhibitor carboxylic group. Essentially identical interactions were observed in the maleate

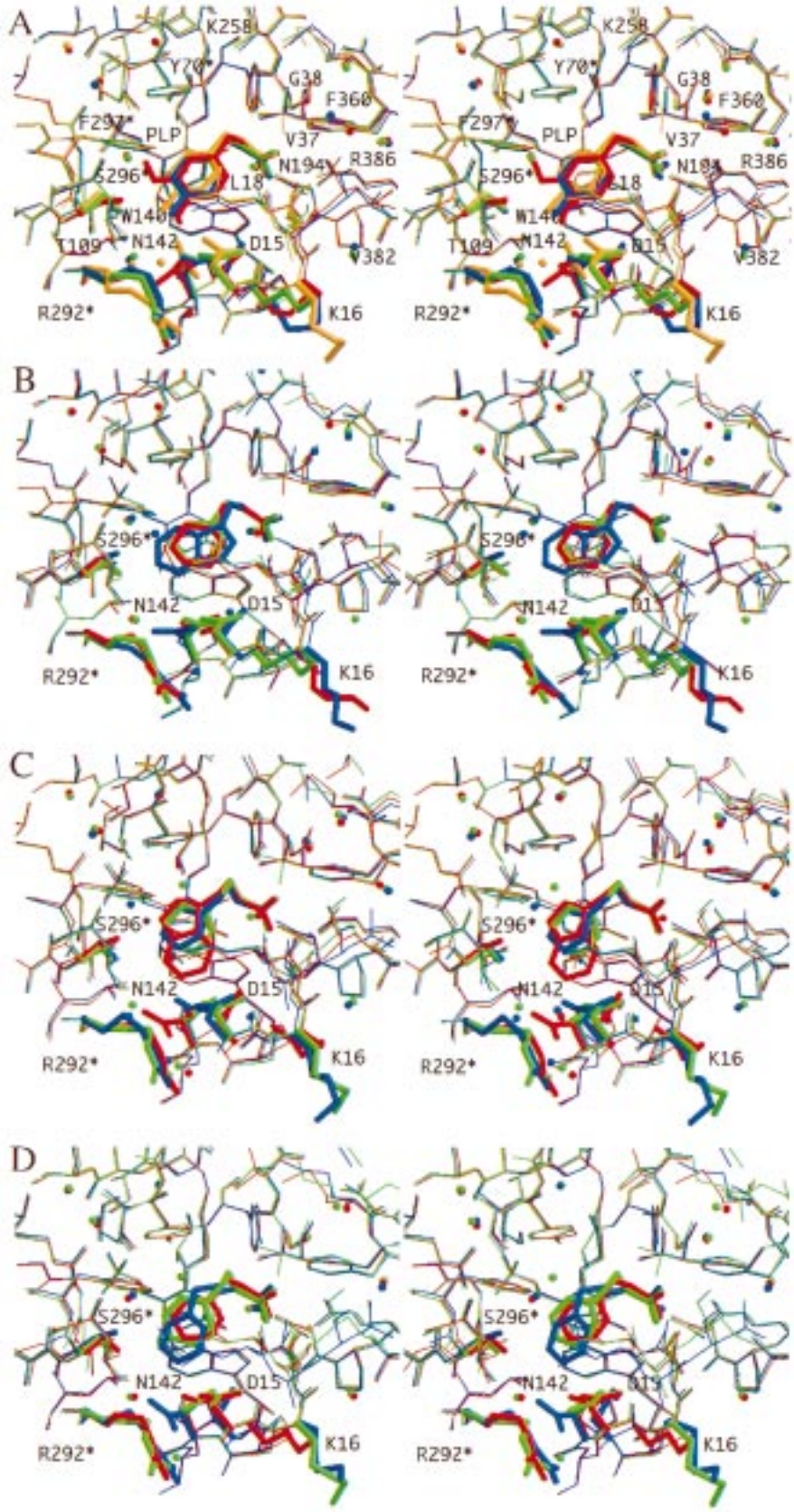

FIGURE 5: Stereoview superimpositions of the active sites. The residues that significantly deviate (side chains of residues 15, 16, 142, 292*, and 296*) and the inhibitors are drawn by a thick line. (A) Superimpositions of PP (green), PTP (blue), AHC (orange), and DMP (red) complexes. (B) Superimpositions of PP (green), CHP (red), and IP (blue) complexes. (C) Superimpositions of TB (blue), PB (green), and IB (red) complexes. (D) Superimpositions of PP (red), PB (green), and PV (blue) complexes. This figure was generated using the program MORSCRIPT (*26*) and RASTER3D (*27, 28*).

complex of pdAroAT (*5*) and the acidic inhibitor complexes of aspartate aminotransferases (AspAT) (*13*−*17*). In addition, the side chains of Val37 and Trp140 interact with the methylene moieties of the inhibitors.

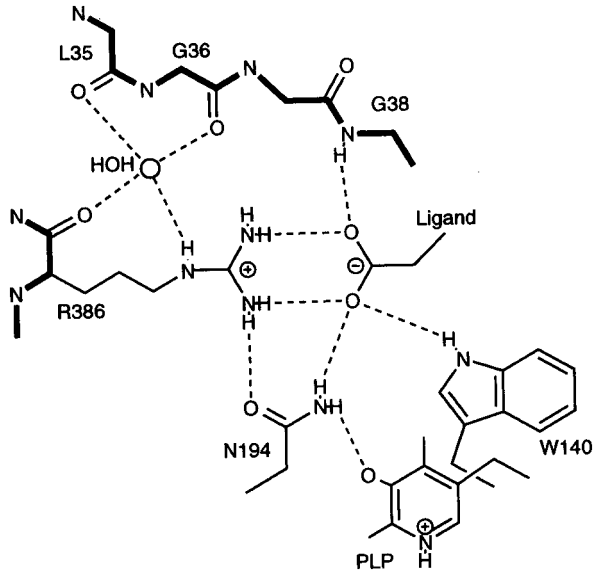

FIGURE 6: Schematic drawing of the binding site for carboxylate of the inhibitors. Main chains are represented by thick lines and hydrogen bonds by broken lines.

In contrast, the residues around the "probing group" of the inhibitors showed significant structural differences in these complexes. The side chain conformations of Asp15, Lys16, Leu18, Asn142, Arg292*, and Ser296* were significant, and the positions of the main chain of residues 15−18 were slightly different (Figure 5). In addition, the number and position of the water molecules around the "probing groups" of the inhibitors were also different.

In the PP complex, the hydrogen bond networks involving Asp15, Lys16, Thr109, Asn142, Arg292*, Ser296*, PLP, and a water molecule were constructed around the phenyl group of PP and played a major role in the recognition of the aromatic side chain of the substrate as previously described (*5*). In the CHP, PTP, TB, and PB complexes, similar hydrogen bond networks were observed around the "probing groups" of the inhibitors. However, the side chain conformations of Asp15, Lys16, Leu18, and Arg292* in these complexes were slightly different from those observed in the PP complex (Figure 5). The "probing groups" of these inhibitors interacted with PLP and the side chains of Asp15, Ile17, Leu18, Tyr70*, Trp140, Asn142, Ser296*, and Phe297* by van der Waals contacts. The area of the van der Waals contact was larger than that observed in the PP complexes. In the TB complexes, the sulfur atom of thienyl group of TB could form a weak hydrogen bond with the hydroxyl group of Tyr70* (3.6 Å).

In the IP, IB, and PV complexes, the hydrogen bond networks observed in the PP complex were broken because of the marked conformational changes of the side chains of Asp15, Asn142, and Ser296*. The "probing groups" of IB and PV made van der Waals interactions with PLP and the side chains of Asp15, Ile17, Leu18, Tyr70*, Thr109, Trp140, Asn142, Arg292*, Ser296*, and Phe297*, and the "probing groups" of IP made van der Waals interactions with the same residues except for Arg292*. Hydrogen bonds between the "probing groups" and the active site residues were not observed.

In the AHC and DMP complexes, the amino group of AHC and two methoxy groups of DMP formed two hydrogen bonds with the side chains of Asn142 and Ser296*, and these new hydrogen bonds disrupted the hydrogen bond networks observed in the PP complex. The "probing groups" of DMP made van der Waals interactions with PLP and the side chains of Asp15, Ile17, Leu18, Tyr70*, Thr109, Trp140, Arg292*, and Phe297* and that of AHC with PLP and the side chains of Asp15, Ile17, Leu18, Tyr70*, Trp140, and Phe297*.

Kinetic analyses of AroATs showed that the free energy differences between the transition state and unbound enzyme plus substrate ($\Delta G_T^{\ddagger}$) were correlated with the ASAs of the inhibitors (*4, 18*−*20*). The ASAs of the inhibitors used in this paper are shown in Figure 1, and obvious correlations were not observed between the $RT\ ln(K_d)$ values of pdAroAT and these ASAs. However, the pattern of the hydrogen bond networks in the active site around the "probing groups" changed according to the size of the ASA of the inhibitors except for the AHC and DMP complexes. For the inhibitors of the ASA < 350 Å^2 (PP, CHP, TB, PB, and PTP), the same hydrogen bond networks were well-constructed, but for the inhibitors of the ASA > 350 Å^2 (IP, PV, and IB), the networks were partially broken. In the AHC and DMP complexes, the hydrophilic substituents on the phenyl rings intercepted the hydrogen bond networks and formed new hydrogen bonds.

DISCUSSION

A comparison of the active site structures of the pdAroAT−inhibitor complexes, especially among the PP, PB, and PV complexes or between the IP and IB complexes, showed that the active sites of pdAroAT would accept the structural differences in the inhibitors at the region that interacts with the "probing groups" of inhibitors by changing the structures of the side chains of the active site residues, while the methylene chains and the carboxylates of the inhibitors were bound to the active site in the same manner in all of these complexes. The heterogeneity of the structural deformations in the active site on binding of the inhibitors suggests that the active site of pdAroAT consists of two parts: the rigid and flexible regions. This observation is consistent with that reported by Kawaguchi et al., which showed the flexible and rigid binding subsites in the active site of AspAT, AroAT, and their chimera from *Escherichia coli* using kinetic analyses for a series of aliphatic substrates (*20*).

The identical spatial arrangements of the carboxylates and the methylene chains of the inhibitors in the complexes suggest that the active site residues interacting with these moieties, including the main chains of the residues 36−38, are structurally rigid in the closed form. Hydrogen bonds and ion pairs play an important role for the binding of the carboxylates. However, during the open−closed conformational change on binding of the inhibitor, the conformations of the main chains of Gly36, Val37, and Gly38 significantly changed (*5*). These contradictory observations suggest that there are two deep energy minima for the conformations of the rigid region of the active site, "open form" and "closed form", and that the conversion from the open to closed form is triggered by binding of the inhibitor. The same type of conversion in the conformation of residues 36−38 on binding of the inhibitor was also observed in the AspATs (*14, 15, 17, 21*−*23*). In the transamination reaction with the amino

acid substrate, the enzyme must abstract the proton from the C_α atom of the substrate. For easy removal of the α-hydrogen, the C_α-H bond of the substrate should be fixed perpendicular to the π system of the pyridine ring of PLP (*24*). The fact that the interactions of the carboxyl groups and aliphatic moieties of the inhibitors with rigid active site regions were essentially identical in all the enzyme−inhibitor complexes showed that such an interaction should be necessary for the substrate to be properly fixed for the efficient catalytic reaction.

Flexibility of the "probing groups" binding site was based on the conformational versatility of the side chains of Asp15, Lys16, Asn142, Arg292*, and Ser296*. The similar conformational versatility also plays a major role in switching the substrate specificity between the acidic and aromatic substrates in pdAroAT (*5*). Especially the high *B* factors (>50 Å^2) of residues 15−18 indicated the dynamic flexibility of these residues in the complexes (data not shown). Except for the AHC and DMP complexes, the "probing group" interacted with the active site residues by only van der Waals interactions which has nondirective and short-range properties. The high flexibility of the active site residues maximizes the van der Waals interactions between the "probing group" and the active site to fit the shape of the active site into that of the "probing group".

Morton et al. investigated the role of the shape complementarity in ligand binding using a cavity-containing mutant of T4 lysozyme and mainly nonpolar ligands (*2*, *3*). They analyzed the binding reaction by dividing it into three distinct processes, in which the binding energy consisted of the free energies of transfer, statistics for the immobilization of the ligand, and packing. The packing free energy was further divided into the free energies of reorganization of the protein and interaction between the protein and ligand. They concluded that the various structural reorganizations observed in the complexes were roughly isoenergetic and that the differences in the free energy of packing were ascribed to the difference in the free energy of the interaction between the protein and ligand. The X-ray analysis showed that the cavity of the mutant T4 lysozyme consisted of two parts, the relatively rigid and more flexible regions. The flexible regions of the cavity changed the conformation according to the shapes of the ligands. The active site of pdAroAT also has rigid and flexible regions, but its structural features are very different from that of the cavity of the mutant T4 lysozyme. The cavity of the mutant T4 lysozyme is constructed with only the hydrophobic side chain, whereas half of the active site cavity of pdAroAT is constructed with the hydrogen bond networks.

The hydrogen bond networks observed in the active site of pdAroAT were partially broken when the inhibitor with ASA greater than 350 Å^2 was bound to the active site. For a detailed analysis, the active site structures of the PP (309.6 Å^2 of ASA) and IP (352.4 Å^2) complexes were compared. PP and IP have a common structure, the propionic acid, and the ASA of IP is larger than that of PP by 42.8 Å^2. Oue et al. showed that $\Delta G_T^{\ddagger}$ correlates with the ASA of the inhibitors and that $\Delta G_T^{\ddagger}$ per Å^2 is estimated to be −0.25 kJ mol^{-1} Å^{-2} for the straight-chain aliphatic amino acids (*4*). Simple application of this value predicts that IP should bind with pdAroAT about 75 times stronger than PP do ($\delta\Delta G_T^{\ddagger}$ = −10.7 kJ mol^{-1}). However, the K_d values of IP and PP were almost identical (Table 3). The X-ray analyses showed that, in the IP complex, the hydrogen bond networks observed in the PP complex were partially broken. Fersht et al. estimated that one hydrogen bond between the ligand and protein contributes 2.1−6.3 kJ mol^{-1} (*25*). The energy loss caused by the breakages of several hydrogen bonds would be compensated by the van der Waals interactions with the bulky "probing group" of the inhibitor in the IP complex of pdAroAT. Further analyses of the hydrogen bond networks in the active sites of all enzyme−inhibitor complexes showed that, although the reorganization of the active site structures of pdAroAT on binding of the inhibitors with the ASA less than 350 Å^2 may be isoenergetic, the breaking of some of the hydrogen bonds upon binding of the inhibitors with the ASA greater than 350 Å^2 would cost extra energy for the reorganization of the active site structure. pdAroAT can catalyze the transamination reaction with not only the aromatic but also the acidic substrate (*4*). If pdAroAT has a completely hydrophobic active site, it would not be able to bind the acidic substrate with only a slight reorganization of the active site structure (*5*). This may be the reason that pdAroAT uses the hydrophilic active site for the recognition of the hydrophobic substrate despite the energy loss by the hydrogen bond breakage.

In summary, the active site of the pdAroAT consists of relatively rigid and more flexible regions as shown previously in the artificial ligand-binding site of the mutant T4 lysozyme. The rigidity and flexibility of the active site structure would play an important role in the functions of these regions. This paper would be a useful guidance for the new design of substrate recognition sites of the enzyme.

REFERENCES

1. Gerstein, M., Lesk, A. M., and Chothia, C. (1994) *Biochemistry 33*, 6739−6749.
2. Morton, A., and Matthews, B. W. (1995) *Biochemistry 34*, 8576−8588.
3. Morton, A., Baase, W. A., and Matthews, B. W. (1995) *Biochemistry 34*, 8564−8575.
4. Oue, S., Okamoto, A., Nakai, Y., Nakahira, M., Shibatani, T., Hayashi, H., and Kagamiyama, H. (1997) *J. Biochem. 121*, 161−171.
5. Okamoto, A., Nakai, Y., Hayashi, H., Hirotsu, K., and Kagamiyama, H. (1998) *J. Mol. Biol. 280*, 443−461.
6. Higashi, T. (1990) *J. Appl. Crystallogr. 23*, 253−257.
7. Brünger, A. T. (1992) *X-PLOR (Version 3.1) − A system for X-ray crystallography and NMR*, Yale University Press, New Haven, CT.
8. Engh, R. A., and Huber, R. (1991) *Acta Crystallogr., Sect. A 47*, 392−400.
9. McRee, D. E. (1992) *J. Mol. Graphics 10*, 44−47.
10. Luzzati, V. (1952) *Acta Crystallogr. 5*, 802−810.
11. Shrake, A., and Rupley, J. A. (1973) *J. Mol. Biol. 79*, 351−371.
12. Kabsch, W., and Sander, C. (1983) *Biopolymers 22*, 2577−2637.
13. McPhalen, C. A., Vincent, M. G., and Jansonius, J. N. (1992) *J. Mol. Biol. 225*, 495−517.
14. Okamoto, A., Higuchi, T., Hirotsu, K., Kuramitsu, S., and Kagamiyama, H. (1994) *J. Biochem. 116*, 95−107.
15. Jäger, J., Moser, M., Sauder, U., and Jansonius, J. N. (1994) *J. Mol. Biol. 239*, 285−305.
16. Malashkevich, V. N., Strokopytov, B. V., Borisov, V. V., Dauter, Z., Wilson, K. S., and Torchinsky, Y. M. (1995) *J. Mol. Biol. 247*, 111−124.

17. Rhee, S., Silva, M. M., Hyde, C. C., Rogers, P. H., Metzler, C. M., Metzler, D. E., and Arnone, A. (1997) *J. Biol. Chem. 272*, 17293−17302.
18. Hayashi, H., Inoue, K., Nagata, T., Kuramitsu, S., and Kagamiyama, H. (1993) *Biochemistry 32*, 12229−12239.
19. Onuffer, J. J., Ton, B. T., Klement, I., and Kirsch, J. F. (1995) *Protein Sci. 4*, 1743−1749.
20. Kawaguchi, S., Nobe, Y., Yasuoka, J., Wakamiya, T., Kusumoto, S., and Kuramitsu, S. (1997) *J. Biochem. 122*, 55−63.
21. Kirsch, J. F., Eichele, G., Ford, G. C., Vincent, M. G., Jansonius, J. N., Gehring, H., and Christen, P. (1984) *J. Mol. Biol. 174*, 497−525.
22. McPhalen, C. A., Vincent, M. G., Picot, D., Jansonius, J. N., Lesk, A. M., and Chothia, C. (1992) *J. Mol. Biol. 227*, 197−213.
23. Hohenester, E., and Jansonius, J. N. (1994) *J. Mol. Biol. 236*, 963−968.
24. Dunathan, H. C. (1966) *Proc. Natl. Acad. Sci. U.S.A. 55*, 712−716.
25. Fersht, A. R., Shi, J. P., Knill, J. J., Lowe, D. M., Wilkinson, A. J., Blow, D. M., Brick, P., Carter, P., Waye, M. M., and Winter, G. (1985) *Nature 314*, 235−238.
26. Kraulis, P. J. (1991) *J. Appl. Crystallogr. 24*, 946−950.
27. Bacon, D. J., and Anderson, W. F. (1988) *J. Mol. Graphics 6*, 219−220.
28. Merritt, E., and Murphy, M. E. P. (1994) *Acta Crystallogr., Sect. D 50*, 869−873.

BI981921D